JGR Atmospheres

RESEARCH ARTICLE
10.1029/2022JD036600

Key Points:

- Following the Raikoke eruption, a layer of sulfate aerosols developed in the stratosphere over northern latitudes, persisting for months
- Aerosol composition and physical properties were derived from measurements by the Atmospheric Chemistry Experiment
- No evidence of stratospheric smoke was found in the Arctic region, contradicting previous reports

Supporting Information:

Supporting Information may be found in the online version of this article.

Correspondence to:

C. D. Boone,
cboone@scisat.ca

Citation:

Boone, C. D., Bernath, P. F., Labelle, K., & Crouse, J. (2022). Stratospheric aerosol composition observed by the Atmospheric Chemistry Experiment following the 2019 Raikoke eruption. *Journal of Geophysical Research: Atmospheres*, *127*, e2022JD036600. https://doi.org/10.1029/2022JD036600

Received 4 FEB 2022
Accepted 13 SEP 2022

Author Contributions:

Conceptualization: Chris D. Boone
Formal analysis: Chris D. Boone
Methodology: Chris D. Boone
Resources: Keith Labelle
Software: Chris D. Boone
Supervision: Peter F. Bernath
Visualization: Jeff Crouse
Writing – original draft: Chris D. Boone
Writing – review & editing: Peter F. Bernath, Keith Labelle, Jeff Crouse

Stratospheric Aerosol Composition Observed by the Atmospheric Chemistry Experiment Following the 2019 Raikoke Eruption

Chris D. Boone[1], Peter F. Bernath[1,2,3], Keith Labelle[3], and Jeff Crouse[1]

[1]Department of Chemistry, University of Waterloo, Waterloo, ON, Canada, [2]Department of Chemistry and Biochemistry, Old Dominion University, Norfolk, VA, USA, [3]Department of Physics, Old Dominion University, Norfolk, VA, USA

Abstract Infrared aerosol spectra derived from Atmospheric Chemistry Experiment measurements following the June 2019 Raikoke volcanic eruption are used to evaluate the composition of stratospheric aerosols in the Arctic. A blanket of aerosols, spanning an altitude range from the tropopause (8–11 km) to 20 km, persisted in the stratosphere over northern latitudes for many months. The aerosols within this blanket were almost exclusively sulfates. The percentage of sulfuric acid in the aerosols decreased over time, dropping below 50% H_2SO_4 concentration at some altitudes by March 2020. Contrary to previous reports, the aerosol blanket was not comprised of smoke particles.

Plain Language Summary Particles in the atmosphere were measured from a satellite-based instrument following the 2019 eruption of the Raikoke volcano. These particles were found to be predominately liquid droplets containing a mixture of sulfuric acid and water. A thick blanket of the particles settled over northern regions and lasted for months. Contrary to previous reports, particles in this blanket did not consist of smoke from intense fires that occurred shortly after the volcano's eruption.

1. Introduction

Stratospheric aerosols play an important role in the Earth's atmosphere, impacting climate through interaction with radiation (e.g., Christian et al., 2019; Kremser et al., 2016; Oman et al., 2005; Sellitto, di Sarra, et al., 2016) and atmospheric chemistry through heterogeneous reactions on the surface of aerosol particles (e.g., Hofmann & Solomon, 1989; Solomon et al., 1986). Aerosol composition plays a significant role in both processes, determining the optical properties of the aerosol, along with the nature and efficacy of heterogeneous reactions.

Launched in 2003, the Atmospheric Chemistry Experiment (ACE) is a satellite-based mission for remote sensing of the Earth's atmosphere (Bernath, 2017). It uses the solar occultation measurement technique, collecting a series of measurements through the Earth's atmosphere as the Sun rises or sets from the orbiting satellite's perspective, providing up to 30 measurement opportunities per day. The primary instrument on board is the Atmospheric Chemistry Experiment Fourier Transform Spectrometer (ACE-FTS), featuring high resolution (0.02 cm^{-1}, unapodized), broad spectral coverage (750–4,400 cm^{-1}), and a signal-to-noise ratio ranging from ~100:1 up to ~400:1 (Buijs et al., 2013). There is also a pair of filtered imagers on board, providing atmospheric extinction profiles at 527.11 and 1,020.55 nm (Gilbert et al., 2007).

The primary purpose of the ACE-FTS instrument is the retrieval of volume mixing ratio (VMR) profiles for gas phase molecules. The most recent processing version (Boone, Bernath, Cok, et al., 2020) provides information on 44 molecules and 24 subsidiary isotopologues, including several molecules whose concentrations are perturbed when atmospheric aerosol levels are enhanced (e.g., SO_2, CO, C_2H_6, HNO_3, H_2O) (Boone, Bernath, & Fromm, 2020; Doeringer et al., 2012). Correlations between these molecular perturbations and aerosol observations allows a measure of internal consistency.

ACE-FTS transmittance spectra contain information on both gas phase molecules and condensed phase particles (e.g., clouds and aerosols) along the line of sight. The infrared spectrum corresponding to condensed phase particles can be generated by dividing out a calculated spectrum containing all known gas phase contributions to the measurement (Boone, Bernath, & Fromm, 2020). The infrared region is well suited for determining aerosol composition (Clarisse et al., 2013; Guermazi et al., 2021; Rinsland et al., 1994). Vibrational spectral features in the infrared are typically strong and rich in structure (Boone, Bernath, & Fromm, 2020; Doeringer et al., 2012),

distinctive for a particular aerosol type, often permitting one to identify composition at a glance. In addition, optical constants (real and imaginary index of refraction as a function of wavenumber) derived from laboratory measurements (Lund Myhre et al., 2003) can be used to determine physical properties of aerosols through analysis of the infrared spectrum (Doeringer et al., 2012; Guermazi et al., 2021).

The Raikoke volcano (latitude 48.3°N, longitude 153.3°E) on the Kuril Islands in the western Pacific Ocean started erupting 21 June 2019, injecting a plume directly into the stratosphere, with cloud tops reaching at least 14 km and rising more than 6 km over a span of 4 days following the eruption (Muser et al., 2020). A portion of the plume separated out and moved equatorward (Gorkavyi et al., 2021) (referred to hereafter as the southern branch), its horizontal transport likely facilitated by atmospheric circulation associated with the Asian monsoon anticyclone (Kloss et al., 2021). The southern branch likely mixed with plumes from the Ulawun (latitude 5.1°S, longitude 151.3°E) eruption on 26 June (Kloss et al., 2021). Material in the main plume spread longitudinally and was transported poleward (Gorkavyi et al., 2021), presumably by the Brewer-Dobson circulation.

Aerosol optical depth at high northern latitudes was elevated for up to a year following the Raikoke eruption (Kloss et al., 2021). Observations by the Cloud-Aerosol Lidar and Infrared Pathfinder Satellite Observations (CALIPSO) satellite (Kim et al., 2018) generally designated stratospheric aerosols during this time period as sulfate (Ohneiser et al., 2021). Lidar measurements from the 1-year MOSAiC (Multidisciplinary drifting Observatory for the Study of Arctic Climate) expedition through the Arctic Ocean on board a German icebreaker suggested the aerosols were smoke rather than sulfate (Ohneiser et al., 2021), prompting a call for the revision of years' worth of sulfate identifications from the CALIPSO mission (Ansmann et al., 2021). Implementing such a change would impact many published studies, and it therefore becomes crucial to verify the composition of aerosols at high northern latitudes in the wake of the Raikoke eruption.

It is worth noting that it is challenging to unambiguously determine composition using the small set of shortwave measurements provided by lidar (Osborne et al., 2022). Lidar measures light from the instrument's laser scattered back into the detector by atmospheric aerosols and clouds. The ratio of scattered light at different wavelengths can provide insight into composition, but the range of natural variability of physical characteristics (size distribution, shape, relative amounts of various components…) for different aerosol types can yield overlap in spectral response, potentially complicated by multiple scattering for efficient scatterers (Chen et al., 2002; Ma et al., 2017). This leads to the potential for misidentification that will depend on the parameter boundaries selected to delineate different aerosol types (Kim et al., 2018). External cues can be adopted, such as location or time of year, to assess the most likely classification (Kim et al., 2018), but this has limitations if a measured scene consists of multiple aerosol types or if the spectral response from the aerosols falls outside the range of expectations (Kanitz et al., 2014). Depolarization of light can be used to discriminate between spherical (typically liquid droplet) and irregularly shaped aerosols (Gasteiger & Freudenthaler, 2014), but some solid aerosols could become glassy (Murphy et al., 2021), potentially yielding lower depolarization ratios in scattered light (Ohneiser et al., 2021).

The differing aerosol identifications by CALIPSO and MOSAiC are both necessarily predicated on assumptions. For the CALIPSO identification, sulfate classification results mostly from minimal depolarization ratios in their lidar measurements, suggestive of liquid droplets, with recent volcanic activity providing implicit verification. The underlying assumption was that smoke particles would have an irregular shape and therefore should exhibit higher depolarization ratios than spherical droplets (Sun et al., 2013). Classification as smoke by MOSAiC was based on spectral response in lidar backscatter signals being more consistent with previous observations of smoke, with the assumption that no configuration of sulfate aerosol (i.e., the combination of size distribution, temperature, and H_2SO_4 mixing ratio) could give rise to the same response. Intense fire activity in the Northern Hemisphere provides a potential source for the smoke particles.

Previous observations of SO_2 by the ACE-FTS (Cameron et al., 2021) showed that Raikoke-induced enhancements in SO_2 at high latitudes persisted at least into October 2019. This would seem to argue for sulfate aerosols, in that conversion of SO_2 to H_2SO_4 feeds the formation of this aerosol type. However, when there is an alternate potential source of aerosols, arguing that all (or most) of the enhanced aerosols are sulfate because SO_2 is elevated would itself be an assumption. Fortunately, direct observation of the aerosol infrared spectrum from ACE-FTS measurements represents a means to determine aerosol composition that does not require assumptions or any form of external validation. In the current study, quantitative analysis of ACE-FTS aerosol infrared spectra is used to evaluate stratospheric aerosols in the Northern Hemisphere following the 2019 Raikoke eruption.

2. Data and Methods

2.1. Calculating Sulfate Aerosol Extinction Spectra

Quantitative analysis of a transmittance spectrum involves fitting the data to the standard Bouguer-Beer-Lambert form (Mayerhofer et al., 2020):

$$Ae^{-\alpha L},$$

where α is the extinction coefficient, L is the effective path length through the medium, and the scaling term A is an arbitrary parameter to account for deviations of the baseline from 1.0 that can result from minor issues during calibration of the transmittance spectrum. The extinction coefficient α, which contains contributions from both absorption and scattering, varies with wavenumber following a pattern distinctive to the aerosol in question, giving rise to a transmittance spectrum whose shape is unique to that particle.

The most simplistic representation of sulfate aerosols is that they are composed of aqueous H_2SO_4 solution, liquid droplet mixtures of H_2SO_4 and H_2O. Thus, laboratory measurements of optical constants for aqueous H_2SO_4 can be used to calculate extinction coefficients for sulfate aerosols, permitting a quantitative analysis of ACE-FTS measurements.

Lund Myhre et al. (2003) provided optical constants for different solutions of H_2SO_4 and H_2O over a wide range of temperature (T) and wt% H_2SO_4 (the percentage of H_2SO_4 by weight). These were used to calculate extinction coefficient as a function of wavenumber for a set of physical characteristics using IDL programs made available by the Earth Observation Data Group from the University of Oxford's Department of Physics (http://eodg.atm.ox.ac.uk/MIE/index.html). Because the particles were assumed to be liquid droplets, they were taken to be spherical. A mono-modal lognormal distribution of the following form (Wrana et al., 2021) was applied:

$$\frac{dN(r)}{dr} = \frac{N_0}{\sqrt{2\pi}\cdot r\cdot \ln(S)}\cdot \exp\left(\frac{-\ln^2\left(\frac{r}{r_{med}}\right)}{2\ln^2(S)}\right),$$

where r is radius, r_{med} is the median radius, S is the spread of the lognormal distribution (i.e., the standard deviation of the distribution in ln[r] space), and N_o is number density, set arbitrarily to 40 particles/cm^3. For each combination of T and wt% H_2SO_4 in the Lund Myhre et al. (2003) data set, extinction coefficient as a function of wavenumber was calculated for r_{med} ranging from 0.1 to 1.0 μm in steps of 0.1 μm at three different values of S (1.1, 1.3, and 1.5). Data in the Lund Myhre et al. (2003) set of optical constants cover the wavenumber range 400–7,500 cm^{-1}, spanning the full range of the ACE-FTS instrument (750–4,400 cm^{-1}).

Note that the true particle density in the plume (N_o) is unknown and cannot be determined independently from effective path length (L in the Bouguer-Beer-Lambert equation). The only independent quantity that can be determined is N_oL, the average column density in the plume, calculated as 40 particles/cm^3 (the assumed value for N_o in the tabulated extinction coefficients) times the fitted effective path length.

Figure 1 shows the calculated extinction coefficient for a variety of the different adjustable parameters (wt% H_2SO_4, T, median radius, and distribution spread) over the wavenumber range of the ACE-FTS instrument. The shape of the sulfate aerosol spectrum is most sensitive to wt% H_2SO_4, as seen in Figure 1a. The series of H_2SO_4-related spectral peaks between 900 and 1,200 cm^{-1} is perhaps the most distinguishing characteristic of sulfate aerosols. Different amounts of H_2O in the aqueous solution yields dramatic changes in the shape of the extinction coefficient in the 3,300–3,400 cm^{-1} range, which provides high accuracy in the determination of wt% H_2SO_4. The spectral feature giving rise to the behavior near 3,350 cm^{-1} is associated with the O-H stretch vibration from liquid H_2O (Biermann et al., 2000), growing rapidly in relative intensity as the amount of H_2O in the droplet increases. For further information on the sources of different spectral peaks in sulfate aerosols, see Biermann et al. (2000) and Sellitto and Legras (2016).

As shown in Figure 1b, the shape of the spectrum is only mildly sensitive to temperature, mostly a shift in the locations of spectral peaks. While it is generally possible to determine aerosol temperature from ACE-FTS measurements for reasonably strong signals, in the analysis presented here, T is fixed to the ambient temperature determined from the ACE-FTS pressure/temperature retrieval (Boone, Bernath, Cok, et al., 2020).

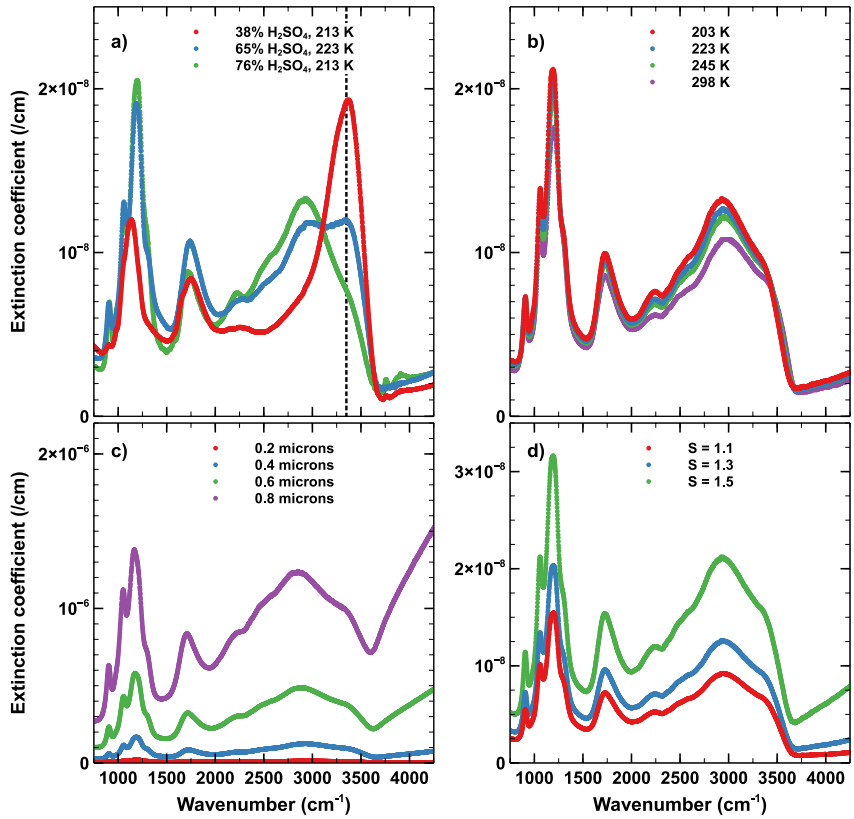

Figure 1. (a) The calculated extinction coefficient for different values of wt% H_2SO_4 at similar temperatures, with median radius = 0.2 μm and distribution spread S = 1.3. The dotted vertical line indicates 3,350 cm^{-1}, the location of a rapidly changing spectral feature. (b) Calculated extinction coefficient for different temperatures, with wt% H_2SO_4 = 72%, median radius = 0.2 μm, and S = 1.3. (c) Extinction coefficient for different values of median radius, with wt% H_2SO_4 = 72%, T = 213 K, and S = 1.3. (d) Extinction coefficient for different distribution spreads, with wt% H_2SO_4 = 72%, T = 213 K, and particle size = 0.2 μm. Note the different vertical scales in the different panels.

From Figure 1c, the magnitude of the extinction coefficient is extremely sensitive to median radius, but the shape of the spectrum relates more to the scattering component of the extinction than the absorption component. Scattering effects increase with wavenumber, inducing a distinct gradient in extinction coefficient as a function of wavenumber. This gradient increases in magnitude with increasing particle size.

For sulfate aerosols, extinction in the region above ~3,700 cm^{-1} comes almost entirely from scattering (calculated via the real part of the index of refraction). There is minimal absorption in this wavenumber region (the imaginary part of the refractive index is close to zero). In Figure 1c, different slopes in extinction coefficient above 3,700 cm^{-1} indicate that there is sensitivity for determining particle size. Note, however, that median radius and distribution spread are highly correlated. For smaller particles, there is insufficient spectral information in the ACE-FTS wavenumber region to determine both median radius and distribution spread (i.e., the spectrum can be reproduced with near identical quality by fixing one parameter and adjusting the other). Therefore, in the analysis presented here, the distribution spread (S) is arbitrarily fixed to 1.3 and median radius is fitted. It is important to note that changing the assumed value of S will systematically change the fitted value for particle size (using a smaller value of S will make the median radius larger) and for effective path length. Thus, values reported in this study for median radius and column density are not necessarily definitive. Values determined for composition (wt% H_2SO_4), however, are insensitive to the assumed value for S.

Interpolation from the pre-tabulated data is required to calculate the extinction spectrum for specific values of the three adjustable parameters: T, wt% H_2SO_4, and median radius. Each extinction coefficient curve (for a given combination of T and wt% H_2SO_4) is interpolated to the target radius using cubic splines. Bilinear interpolation is then used to complete the calculation, bracketing the target values of T and wt% H_2SO_4 with the four closest points in the pre-tabulated data set (lower T and lower H_2SO_4, lower T and higher H_2SO_4, higher T and higher

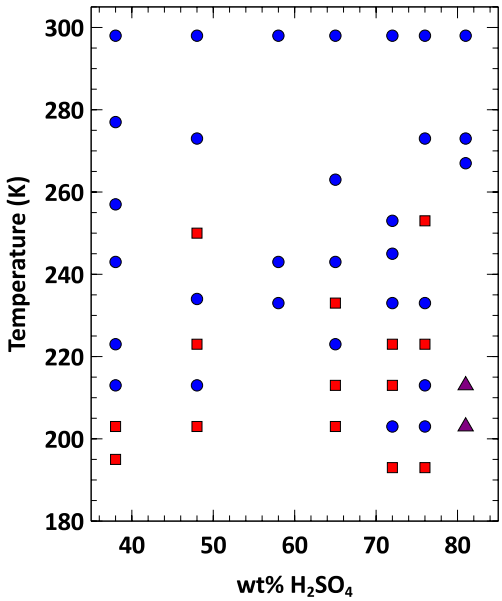

Figure 2. Combinations of temperature and wt% H_2SO_4 in the pre-tabulated data employed in the calculation of sulfate aerosol spectra. Blue circles indicate data calculated using the Lund Myhre et al. (2003) optical constants, red squares indicate data interpolated or extrapolated in temperature, and purple triangles indicate data extrapolated in wt% H_2SO_4.

H_2SO_4, higher T and lower H_2SO_4) in order to interpolate (point-by-point in wavenumber) the extinction coefficient for the given set of aerosol radius, T, and wt% H_2SO_4.

The information in the Lund Myhre et al. (2003) data does not encompass all conditions encountered in the atmosphere. It therefore sometimes becomes necessary to extrapolate in T and/or wt% H_2SO_4. Performing this extrapolation using bilinear interpolation is not ideal, so the tabulated data were extended prior to the analysis. For a given wt% H_2SO_4, extrapolation in T of extinction coefficient (α) is performed (point-by-point in wavenumber) using the following Padé approximant form:

$$\alpha_i(T) = \frac{a_i + b_i\,(T - T_o)}{1 + c_i(T - T_o)^2}$$

where the reference temperature T_o was arbitrarily chosen as 225 K. At each wavenumber point (denoted by the subscript "i"), values for parameters a_i, b_i, and c_i were fitted from the tabulated extinction data, the data calculated from the Lund Myhre et al. (2003) optical constants.

The extended coverage for the tabulated data employed for the calculation of sulfate aerosol spectra is shown in Figure 2. Red squares indicate data that were interpolated to fill in gaps or extrapolated to extend the coverage. Note that for 72% H_2SO_4, the Lund Myhre et al. (2003) optical constants were nearly identical for temperatures 213 and 223 K. The pre-tabulated calculations from both temperatures for 72% H_2SO_4 were therefore excluded from the Padé approximant analysis and subsequently replaced by interpolated data. For 81% H_2SO_4, there were insufficient data points to extrapolate in temperature, so a Padé approximant extrapolation was performed in wt% H_2SO_4 for temperatures 203 and 213 K (indicated by the purple triangles in Figure 2), needed for rare situations where H_2SO_4 exceeds 76%.

Two other sets of optical constants were evaluated for the sulfate aerosol calculation, one by Niedziela et al. (1999) and another by Biermann et al. (2000). Neither of these data sets had the combinations of high H_2SO_4 concentration at low temperatures featured in the Lund Myhre et al. (2003) data set, which were crucial for the analysis of sulfate aerosols under typical atmospheric conditions. With these two data sets, it was necessary to fit for T rather than fixing it to the ambient value, and the least squares fitting would typically converge to the closest temperature for which sufficiently high wt% H_2SO_4 was available, yielding fairly accurate H_2SO_4 concentration but often giving temperatures significantly different from ambient.

2.2. Calibrated ACE-FTS Residual Spectra

The aerosol infrared spectrum in a particular measurement can be isolated by calculating a residual spectrum from ACE-FTS spectra, that is, a point-by-point division of the measured spectrum by a calculated spectrum containing all known gas-phase contributions, as was done previously for the observation of smoke particles from pyrocumulonimbus (pyroCb) events (Boone, Bernath, & Fromm, 2020). Using an additional "clear sky" calibration occultation with aerosols at background levels, one can remove systematic features from the residual spectrum. One major source of systematic features in residual spectra comes from several strong HNO_3 bands that have no available spectroscopic information in the ACE-FTS line list, which is based on HITRAN-16 (Gordon et al., 2017). Because the HNO_3 bands are missing from the calculated spectrum, their contribution in the measured spectrum does not cancel out when generating the residual spectrum. Systematic features also arise from line shape issues such as line mixing and/or speed dependence effects missing from the calculated spectrum (Boone et al., 2011). When molecules giving rise to the systematic features have comparable VMRs in both the aerosol-containing and clear sky occultations, the systematic features will cancel.

Calibration measurements are typically taken from nearby occultations, to ensure similar atmospheric conditions. However, if all nearby occultations also contain aerosols (as is the case in the current study), the calibration measurement is taken from an occultation in a similar location and season from a different year.

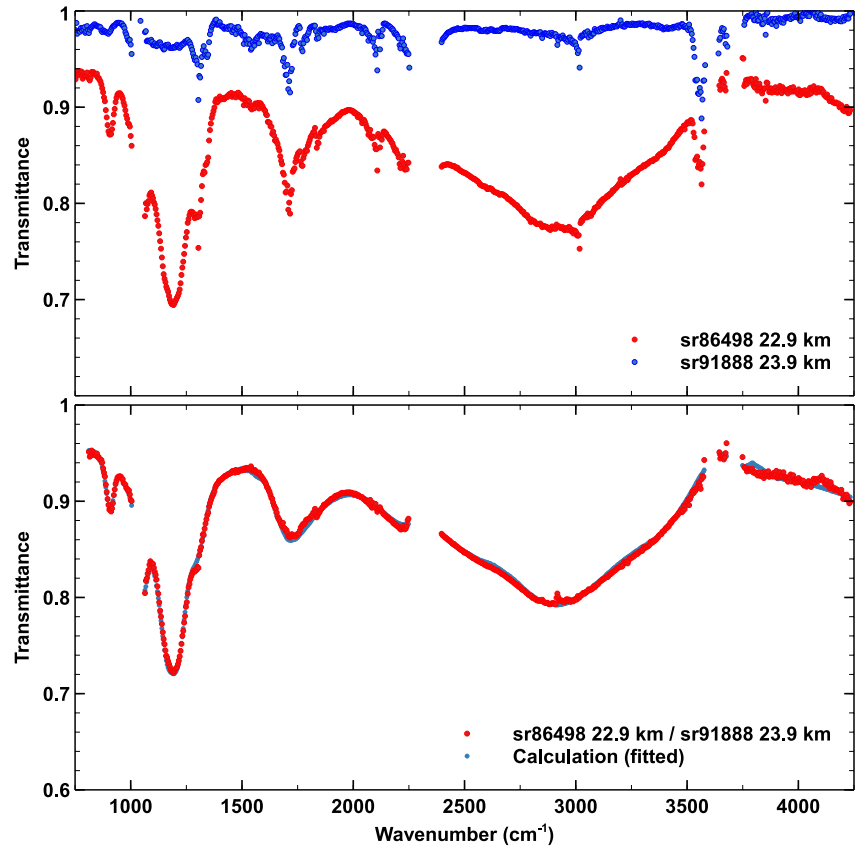

Figure 3. Top panel: in red is the residual spectrum for the measurement at tangent height 22.9 km in occultation sr86498 (2 September 2019, latitude 26.7°N, longitude 48.0°W), and in blue is the residual spectrum for the measurement at tangent height 23.9 km in occultation sr91888 (1 September 2020, latitude 26.7°N, longitude 52.1°W). Bottom panel: In red is the ratio of the two residual spectra from the top panel, and in blue is the calculated sulfate aerosol spectrum, using parameters determined from a least-squares fitting.

Figure 3 shows an example of the calibration process. The top panel shows the residual spectra for an occultation that measured a plume in the Raikoke southern branch (sr86498, where "sr" stands for sunrise and 86,498 is the orbit number, creating a unique identifier for the occultation), and an occultation from the following year and near the same time and location (sr91888). The measurement at 23.9 km in sr91888 is taken under clear sky conditions. Ideally, this calibration measurement would be relatively flat, but it contains a number of spectral features, including several arising from the missing HNO_3 bands in the calculated gas phase spectrum. These features also appear in the measurement at 22.9 km in sr86498 and will therefore cancel out when performing a point-by-point division of the two residual spectra. Gaps in the spectra are regions where the gas phase spectrum saturates and therefore cannot be divided out (to avoid dividing by a number close to zero).

Note that the clear sky measurement also contains sulfate aerosol spectral features at background levels, much weaker than the sulfate aerosol spectrum in the volcanic plume. For the results presented in the current study, the impact of background sulfate aerosol spectra in calibration measurements is small, potentially yielding a slight distortion in the shape of calibrated spectra, particularly for occultations measured a long time after the eruption, when sulfate aerosols are returning toward background levels. Future refinements of the analysis method will account for background sulfate aerosols in the clear sky measurement when generating the calibrated residual spectrum.

The bottom panel in Figure 3 shows the results of a nonlinear least-squares analysis of the calibrated spectrum. With the distribution spread (S) fixed to 1.3, the fitted parameters are as follows: wt% H_2SO_4 = 74.8 ± 0.4%, radius = 0.322 ± 0.006 μm, average column density $N_oL = (1.48 \pm 0.08) \times 10^8$ particles/cm^2, and baseline scaling $A \approx 1$ (within the error bars). Reported uncertainties are the random fitting errors from the least-squares analysis (the square root of the diagonal elements of covariance matrix) and do not include systematic contributions.

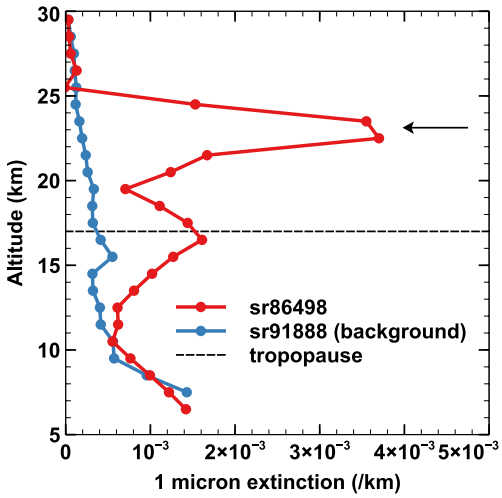

Figure 4. Atmospheric extinction profiles for sr86498 and sr91888. Information on time and location for the two occultations is provided in the caption to Figure 3. The dashed line indicates the location of the tropopause for sr86498. The arrow indicates a sharp, distinct aerosol peak in the extinction profile for sr86498.

A true error estimate would include both random and systematic contributions. Unfortunately, determining systematic errors for the analysis presented here is severely limited by lack of knowledge of the size distribution. However, one parameter (wt% H_2SO_4) is insensitive to assumed size distribution. Changing the distribution spread parameter, S, from 1.3 to 1.1 changes wt% H_2SO_4 by 0.1, a fraction of the random fitting error. The parameter is also relatively insensitive to temperature. Recall that T is fixed to the ambient value derived from the analysis of ACE-FTS measurements. T would need to be in error by more than 10 K for the systematic error in wt% H_2SO_4 to exceed the random fitting error, as determined by changing the fixed value of T and refitting for wt% H_2SO_4. ACE-FTS errors on retrieved temperature are typically within 2 K (Sica et al., 2008), suggesting that systematic errors from this source would also be a fraction of the random fitting error. With other potential sources of systematic error (such as the presence of background sulfate spectra in calibration measurements) added in, uncertainties for wt% H_2SO_4 should be conservatively within a factor of two of the random fitting errors reported in this study.

Conversely, the other parameters determined in the analysis (median radius and N_oL) are very sensitive to the assumed value for S. Changing S from 1.3 to 1.1 would change the fitted value for median radius by an order of magnitude more than the random fitting error, indicating that systematic errors likely represent the dominant uncertainty source for this parameter. Although random fitting errors are reported for median radius and N_oL throughout this study, they should viewed as little more than a measure of fitting quality for these two parameters (the smaller the value of the random error relative to the magnitude of the fitted parameter, the better the fit). Only the reported errors for wt% H_2SO_4 should be considered close to representative of the true errors, albeit underestimated.

The fact that the calibrated spectrum in Figure 3 can be reproduced using sulfate aerosol optical constants serves as verification of the composition. Each aerosol type has its own unique extinction spectrum shape in the infrared. It is not possible to reproduce the spectrum of a different aerosol type (such as smoke) using sulfate aerosol optical constants. If a measurement contained spectra from a combination of aerosol types (e.g., both sulfate and smoke), the analysis would only reproduce a portion of the spectral features (those associated with sulfate aerosols).

3. Results

Here we evaluate Northern Hemisphere observations from the ACE mission for the period from shortly following the Raikoke eruption to spring of the following year (July 2019 through March 2020). For convenience, results are presented for a limited latitude range (60–70°N), but similar results would be obtained for any latitude range north of 50°N.

A solar occultation instrument provides limited geographic coverage, measuring over a small latitude range on a given day and shifting slowly in latitude over time (Bernath, 2017). However, with events that extend over a period of months, the ACE-FTS samples a particular latitude region multiple times, providing information on aerosol evolution.

3.1. The 1 Micron Imager

The near infrared imager (measuring at 1,020.55 nm, or roughly 1 micron) on the ACE satellite collects four images per second of the Sun. A row of imager pixels coaligned with the center of the ACE-FTS field of view is used to retrieve atmospheric extinction at 1 micron as a function of altitude (Gilbert et al., 2007). Aerosol enhancements can be identified by viewing the 1 micron imager atmospheric extinction profiles. Figure 4 shows the extinction profile for occultation sr86498, featuring a sharp, distinct peak roughly 4 km in altitude extent near 23 km (indicated by the arrow in Figure 4), roughly 8 km above the tropopause. Also shown is the extinction profile for the clear sky occultation sr91888, to provide a sense of background aerosol extinction for the imager.

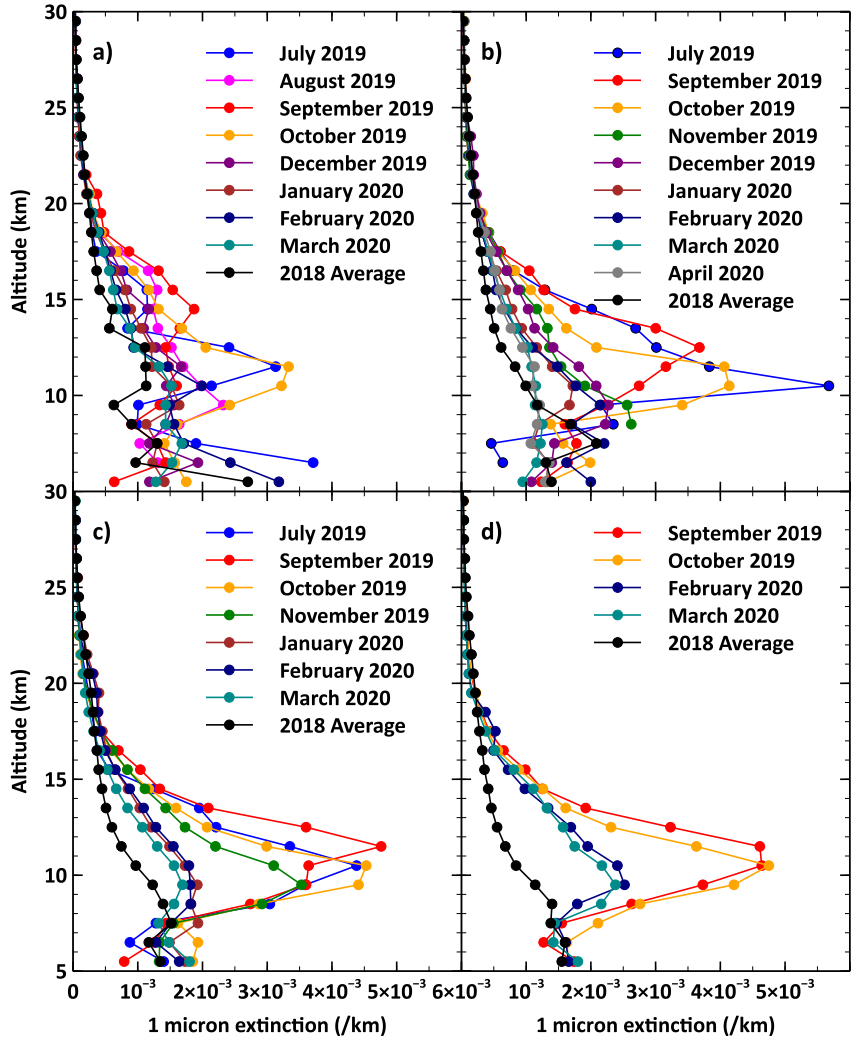

Figure 5. The monthly average 1 micron imager atmospheric extinction for a given latitude range starting in July 2019, which was shortly after the Raikoke eruption. The 2018 yearly average profile is included for reference, to provide a sense of the background extinction level: (a) 40–50°N, (b) 50–60°N, (c) 60–70°N, and (d) 70–85°N. For months lacking a curve, Atmospheric Chemistry Experiment did not measure in the given latitude range during that month.

The aerosol plume at 23 km in sr86498 (from the Raikoke southern branch) was previously identified as sulfate based on the fitting results presented in Figure 3.

Figure 5 shows monthly average atmospheric extinction profiles from the 1 micron imager for the period following the Raikoke eruption, with the 2018 average yearly profile provided for each latitude region as a proxy for background aerosol levels. For all latitude regions north of the Kuril Islands, there is a large injection of aerosols around the time of the Raikoke eruption. Immediately following the eruption, sharp peaks in the imager extinction profiles (similar to Figure 4), 1–4 km in altitude extent and located at a variety of altitudes, indicate a profusion of distinct aerosol plumes. By September 2019, there are no longer distinct plumes in the region north of latitude 50°N, but aerosol levels remain very high, settling into a relatively uniform blanket that extends from near the tropopause up to just below 20 km. This aerosol blanket is illustrated in Figure 6, which plots all of the measured 1 micron imager extinction profiles for October 2019 in the 60 to 70°N latitude region, with imager observations from October 2020 provided for a sense of aerosol background extinction. Tropopause levels for the measurement set in Figure 6 range from 8 to 11 km, and aerosol extinction typically peaks just above the tropopause.

As seen in Figure 5, for latitudes north of 40°N, aerosol enhancements persist at least into April 2020, 10 months after the eruption. There is a sharp drop in aerosol levels with the onset of winter, with sedimentary losses in the

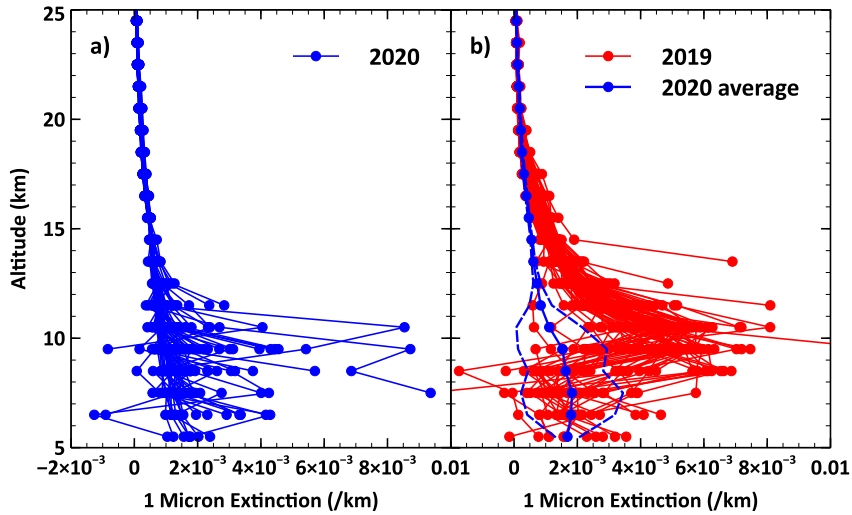

Figure 6. 1 micron imager atmospheric extinction profiles for the time period 21–31 October in the latitude range 60–70°N. (a) All results from 2020 for this time period and region. (b) All results from 2019 in red and the average of 2020 results (the average profile from panel a) in blue, with the standard deviation of the 2020 results indicated by the dashed blue lines.

Arctic potentially accelerated by the descent of air within the polar vortex. Aerosol levels then slowly decline over the remainder of the winter and into spring. Every ACE-FTS measurement north of 50°N from July 2019 through April 2020 contains enhanced aerosols.

Long-lived enhancement in aerosol levels is also observed for latitudes below 40°N (not shown in Figure 5), almost to the tropics, but the level of enhancement at lower latitudes is smaller. For latitudes below 40°N, distinct aerosol peaks like the one in Figure 4 persist into October 2019. In this latitude region, the altitudes of the highest peaks observed by ACE rise steadily over time, suggestive of upward transport, reaching as high as 25 km in October 2019.

3.2. SO_2

When deducing aerosol composition, VMR information from the ACE-FTS is available as complementary information. If the massive aerosol blanket was comprised of smoke particles, as suggested by Ohneiser et al. (2021), one might expect to see enhancements in biomass burning products such as HCN, CO, C_2H_6, and other such molecules measured by ACE (Boone, Bernath, & Fromm, 2020). In the months following the Raikoke eruption, the ACE-FTS captured isolated instances of stratospheric enhancements (relative to other years) in gases associated with biomass burning, but no such enhancements were observed for latitudes greater than 60°N. See Figure S1 in Supporting Information S1 and the associated discussion in the supplementary information provided with this article, which shows results in the 60–70°N latitude region for HCN, a long-lived biomass burning by-product.

On the other hand, every ACE-FTS occultation in the Arctic exhibited enhanced SO_2 levels for several months following the Raikoke eruption (Cameron et al., 2021). Figure 7 tracks SO_2 levels over time in the 60 to 70°N latitude region (the region containing the highest density of measurements for the ACE-FTS) from July 2019 through February 2020. SO_2 falls below the detection limit for the Ozone Mapping and Profiler Suite (OMPS) nadir mapper sensor roughly 2 months after the Raikoke eruption (Gorkavyi et al., 2021), but the sensitivity afforded ACE by measuring in the limb allows the tracking of SO_2 over a longer period of time.

In Figure 7a, the SO_2 VMR profiles are a profusion of distinct peaks at different altitudes, strongly correlated with peaks in the imager profiles. By September (Figure 7b), there are no longer sharp, distinct peaks, but there remains strong enhancement over a broad altitude range, from the tropopause up to ~20 km. This correlates well with the behavior observed in the imager extinction profiles (Figure 6). SO_2 levels continue to drop over time but remain elevated through November 2019 (Figure 7d), over the same altitude range of elevated aerosols indicated by the imager results, falling close to background levels by January 2020 (Figure 7e).

In February 2020 (Figure 7f), increased SO_2 enhancement is observed, with distinct peaks in the profiles that suggest a relatively fresh source. The most likely explanation appears to be the eruption of the Taal Volcano

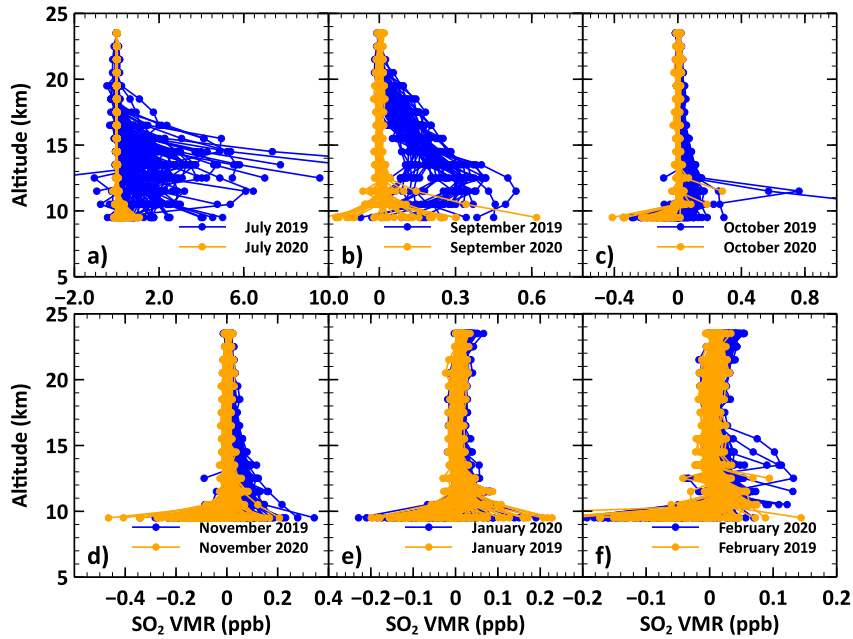

Figure 7. Atmospheric Chemistry Experiment Fourier Transform Spectrometer retrieved SO_2 volume mixing ratio profiles in the 60–70°N region, with blue curves showing the target set and orange curves showing SO_2 spanning the same time period and latitude range from a different year, to provide a sense of background levels. (a) 8–26 July. (b) 12–18 September. (c) 21–31 October. (d) 1–30 November. (e) 11–31 January. (f) 1–20 February. Note the differences in horizontal scale for the different panels.

(latitude 14°N, longitude 120.6°E) on 12 January 2020. The influx of fresh SO_2 in February 2020 was a minor perturbation compared to Raikoke. SO_2 levels in the 60 to 70°N latitude range were again close to background by the time ACE returned to the region in late March 2020 (not shown).

Similar behavior is observed in SO_2 for all other latitude regions north of 50°N, and always correlates well with atmospheric extinction from the 1 micron imager.

3.3. Residual Spectra

Strong correlation between high aerosol levels (implied by the imager extinction profiles) and enhanced SO_2 VMR suggests the presence of sulfate aerosols. However, sulfate aerosols will persist in the stratosphere after SO_2 returns to background levels (Brodowsky et al., 2021). Mild enhancement of SO_2 evident for January in Figure 7e, e.g., constitutes debatable evidence for aerosol composition. Definitive determination of composition requires analyzing the ACE-FTS residual spectra, testing if they can be accurately reproduced using spectroscopic information for a particular aerosol type. The shape of the aerosol spectrum in the infrared provides unambiguous confirmation of aerosol type.

Continuing to focus on the latitude region 60 to 70°N, a series of representative occultations was selected for the months following the Raikoke eruption, to provide a timeline of aerosol evolution. Figure 8 shows the 1 micron imager atmospheric extinction profiles for the selected occultations, along with extinction profiles for 'background occultations' employed to calibrate the residual spectra. Note the changing scale on the *x*-axis in Figure 8. The occultation from July (Figure 8a) contains a distinct plume with a narrow altitude extent. The other panels show measurements from the aerosol blanket that settled over the region, with peak extinctions gradually decreasing over time but remaining significantly above background levels well into March 2020.

Figure 9 shows the results for a measurement with tangent height close to the extinction peak for each occultation. Note the differences in y-scale. In each case, the fitted sulfate spectrum reproduces the calibrated measurement extremely well, verifying the aerosol type as sulfate. Fitting parameters for the calculated spectra in Figure 9 are presented in Table 1.

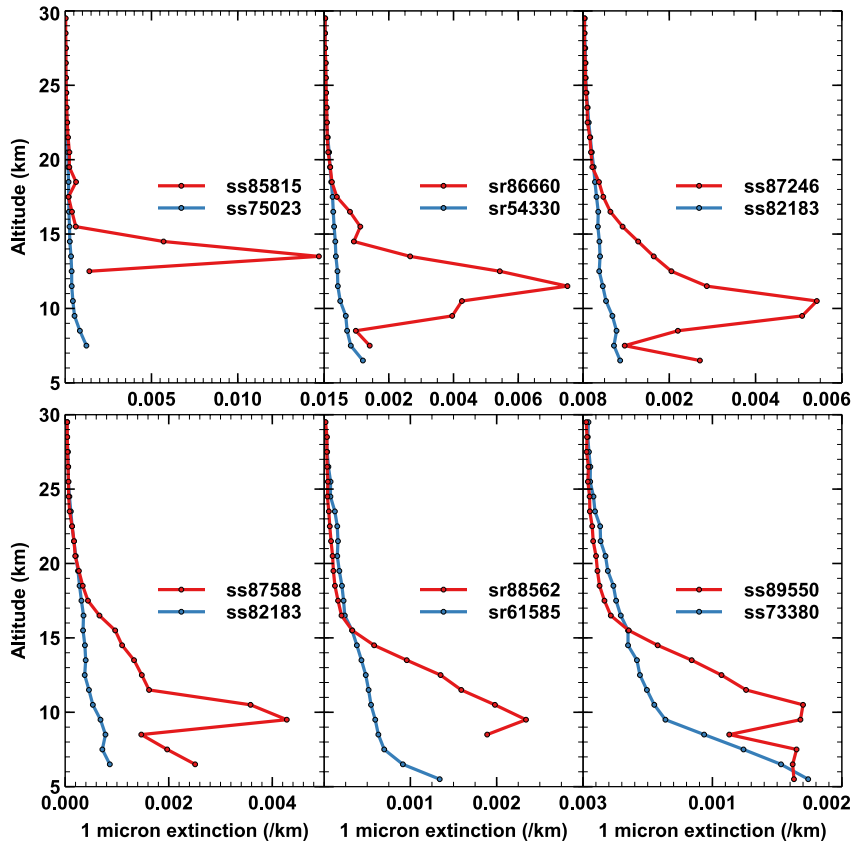

Figure 8. 1 micron imager atmospheric extinction profiles for occultations in the latitude region 60–70°N in the months following the Raikoke volcanic eruption, along with occultations from previous years employed for calibration. (a) ss85815, 18 July 2019, latitude 68.3°N, longitude 63.2°W. (b) sr86660, 13 September 2019, latitude 61.4°N, longitude 43.6°W. (c) ss87246, 23 October 2019, latitude 62.5°N, longitude 129.3°W. (d) ss87588, 15 November 2019, latitude 65.8°N, longitude 146.2°E. (e) sr88562, 20 January 2020, latitude 63.6°N, longitude 83.2°E. (f) ss89550, 27 March 2020, latitude 64.2°N, longitude 109.7°W. Note the differences in horizontal scale for the different panels.

From July 2019 through March 2020, every ACE-FTS occultation measured north of 60°N contains elevated sulfate aerosols. Sulfate aerosol enhancements persist beyond March 2020, but the signal approaches background levels and requires accounting for the sulfate signal in the calibration occultation for proper analysis. The only other stratospheric aerosols observed for this region and time period were polar stratospheric clouds that formed during the winter.

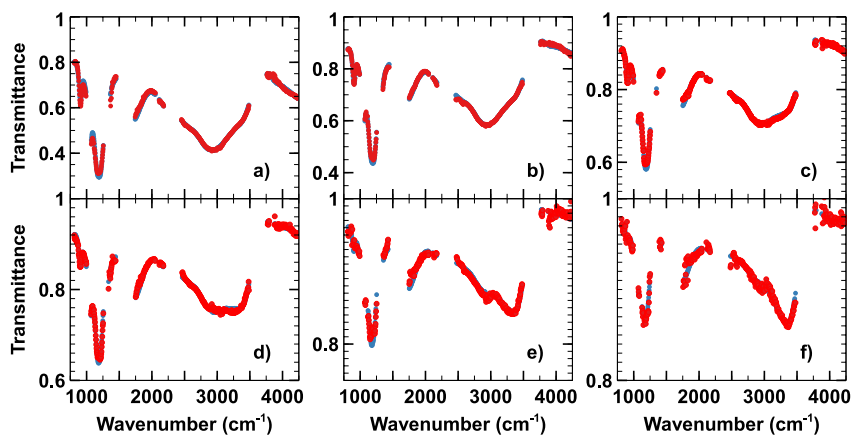

Figure 9. The calibrated measurements (in red) and fitted sulfate spectra (in blue) for: (a) ss85815 12.7 km. (b) sr86660 12.1 km. (c) ss87246 11.0 km. (d) ss87588 10.6 km. (e) sr88562 10.5 km. (f) ss89550 10.3 km. Times and locations for the occultations are provided in the caption to Figure 8. Fitted parameters for the calculated sulfate spectra are provided in Table 1. Note the changing scale on the *y*-axis.

Table 1
Fitting Results for the Spectra Presented in Figure 9

Occultation	Tangent height (km)	wt% H_2SO_4 (%)	Median radius (μm)	Fixed T (K)	N_0L (10^8 particles/cm^2)
ss85815	12.7	73.6 ± 0.2	0.343 ± 0.002	229	4.6 ± 0.1
sr86660	12.1	73.3 ± 0.2	0.238 ± 0.004	227.5	9.6 ± 0.4
ss87246	11.0	68.5 ± 0.3	0.235 ± 0.005	222	6.8 ± 0.4
ss87588	10.6	63.9 ± 0.4	0.247 ± 0.006	218	4.5 ± 0.3
sr88562	10.5	57.3 ± 0.7	0.22 ± 0.01	212	3.8 ± 0.5
ss89550	10.3	53.3 ± 0.8	0.26 ± 0.01	210	1.9 ± 0.3

Note. The distribution spread (S) was set to 1.3 in all cases.

Recall that fitted values for median radius and column density are highly sensitive to the assumed value for distribution spread. No conclusions are drawn for these quantities reported in Table 1, in case size distribution evolved with time rather than remaining roughly constant. However, as mentioned previously, composition (wt% H_2SO_4) is insensitive to the assumed distribution spread S, providing some insight into aerosol evolution over the time frame.

As exemplified by the wt% H_2SO_4 results in Table 1, the fraction of sulfuric acid in the sulfate aerosols (for measurements near the extinction peak just above the tropopause) decreases over time. In Figure 9, this trend is evident from the increasing prominence of the O-H stretch feature near 3,350 cm^{-1}. Note that the composition is far from homogeneous in the aerosol blanket. During a given month, H_2SO_4 could differ by more than 10% at different locations. For nearly all high latitude (>50°N) occultations during this time period, there is also a significant altitude gradient within the aerosol blanket.

Figure 10 shows the measured and fitted spectra for three different tangent heights within a given occultation (ss87246). The 1-micron imager extinction profile for this occultation can be seen in Figure 8, showing a peak in extinction around 10 km. The ability to reproduce measurements at all altitudes within the aerosol blanket with sulfate aerosol spectroscopic information verifies that the entire altitude extent of the blanket is comprised of this aerosol type. Arrows in Figure 10 indicate the location of the O-H stretch spectral feature around 3,350 cm^{-1} that is very sensitive to wt% H_2SO_4, highlighting the changing prominence of this spectral feature with tangent height, providing visual confirmation of the significant altitude gradient in wt% H_2SO_4.

Figure 11 plots the fitted parameters as a function of altitude for 13 measurements in ss87246, spanning 9.2–14.3 km. The plot for wt% H_2SO_4 in Figure 11a shows an increase in sulfuric acid with increasing altitude, ranging from ∼63% at 9.2 km to ∼73% near 14 km. As seen in Figure 11b, the fitted particle size decreases with increasing altitude. Although the fitted radius may have unknown accuracy, dependent as it is on the assumed value for distribution spread (S), the observations clearly indicate higher numbers of larger particles at lower altitudes.

4. Discussion and Conclusions

Following the June 2019 Raikoke eruption, the Northern Hemisphere stratosphere was suffused with aerosols, particularly at higher latitudes. A blanket of stratospheric aerosols settled over northern latitudes and persisted at least into the following spring. Using ACE-FTS residual spectra, it was determined that this blanket was comprised of sulfate aerosols. The ability to accurately reproduce the infrared aerosol spectra using sulfate aerosol optical constants served as incontrovertible proof of aerosol type. ACE-FTS results also showed enhanced stratospheric SO_2 strongly correlated with aerosol extinction, consistent with expectations for sulfate aerosols following a volcanic eruption.

No evidence was found for stratospheric smoke in the Arctic during this time period. This was determined by visual inspection of the fitting results for calibrated residual spectra. The spectra were accurately reproduced using spectroscopic information for sulfate aerosol. If there were also smoke present, there would have been extra spectral features in the measurement, not reproduced by the sulfate optical constants. Also, for latitudes north of 60°N, there were no stratospheric enhancements observed in biomass burning products (e.g., CO, HCN, C_2H_6), molecules that would have been transported into the stratosphere along with the smoke particles (Boone, Bernath, & Fromm, 2020).

The findings reported here contradict previous claims that the aerosol blanket that formed in the high Arctic following the Raikoke eruption was composed almost entirely of smoke particles (Ansmann et al., 2021; Ohneiser et al., 2021). It was not clear what caused the aerosol misclassification from the ground-based results. In our opinion, a lack of similarity in spectral response relative to the plume from a previous volcanic eruption, cited in Ohneiser et al. (2021), is insufficient evidence to exclude sulfate aerosols if the two events gave rise to particles with different composition, median radius, or size distribution.

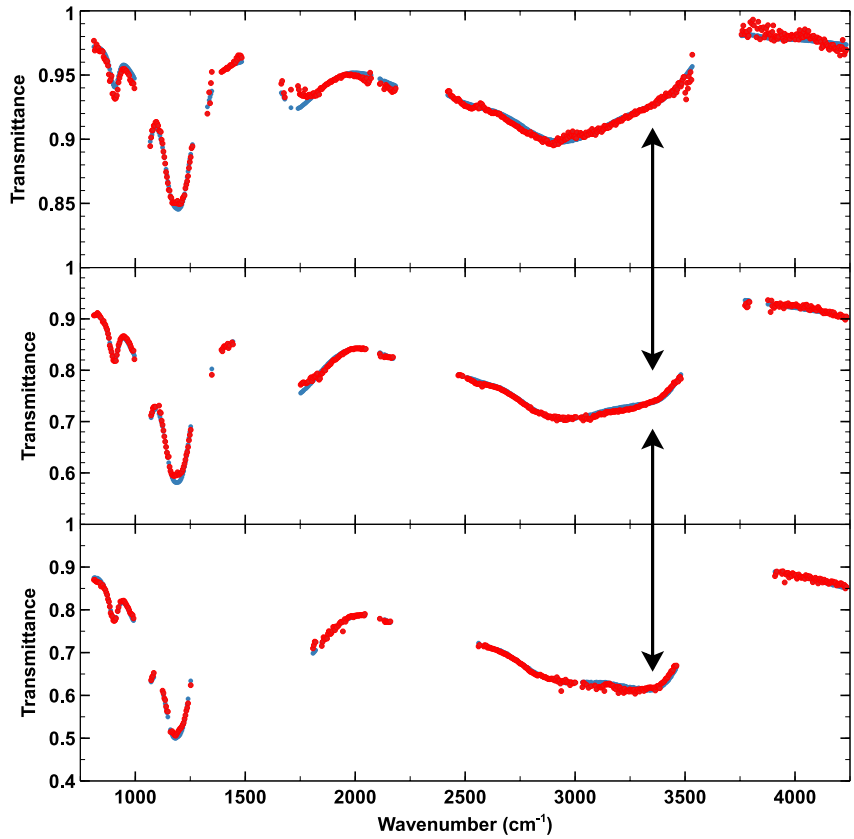

Figure 10. The calibrated spectra (in red) and fitted sulfate aerosol spectra (in blue) for three measurements at different tangent heights in the occultation ss87246 (23 October 2019, latitude 62.5°N, longitude 129.3°W). Top: tangent height = 14.3 km, fitted wt% H_2SO_4 = 73.0 ± 0.7%. Middle: tangent height = 11.0 km, fitted wt% H_2SO_4 = 68.5 ± 0.3%. Bottom: tangent height = 9.5 km, fitted wt% H_2SO_4 = 63.3 ± 0.3%. Arrows indicate the spectral feature most sensitive to changes in wt% H_2SO_4. Distribution spread (S) was set to 1.3 in the analysis.

Altitude gradients in median radius and wt% H_2SO_4 observed in the aerosol blanket could have contributed to the disagreement between CALIPSO observations (probing the aerosol blanket from above) and the MOSAiC results (probing the blanket from below). ACE observations indicate aerosol particles were larger in the lower portion of the blanket and had lower wt% H_2SO_4.

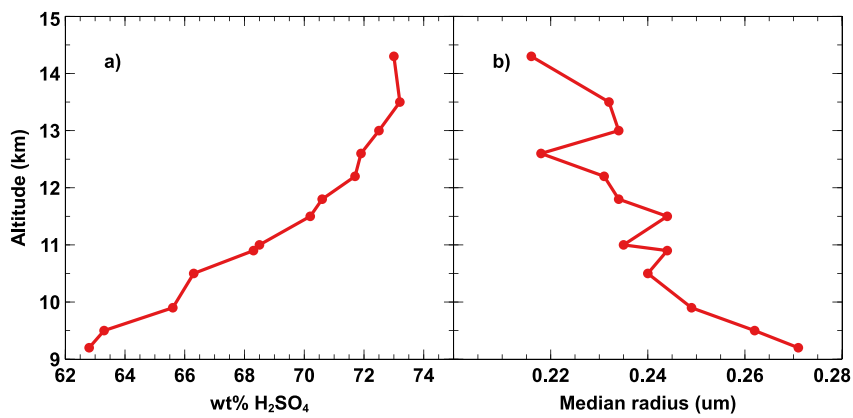

Figure 11. Fitted sulfate aerosol parameters as a function of altitude for occultation ss87246 (time and location information provided in the caption to Figure 10). (a) wt% H_2SO_4. (b) median radius.

Results reported here for the Raikoke eruption may not vindicate other instances of CALIPSO classification called into question by Ansmann et al. (2021). To be rigorous, other CALIPSO findings of sulfate aerosols would need to be evaluated individually. However, the agreement between ACE-FTS and CALIPSO for sulfate aerosols from the Raikoke eruption suggest that a complete overhaul of the CALIPSO classification scheme is likely not warranted. The long data record of the ACE-FTS should provide many opportunities for evaluating aerosol classifications derived by CALIPSO or other instruments on the basis of information from a limited set of wavelengths.

In the Raikoke southern branch at low latitudes, Knepp et al. (2021) use SAGE III aerosol measurements (9 data points at near-infrared, visible, and ultraviolet wavelengths) to classify many aerosols above 20 km as smoke. Absorption by black carbon in smoke particles was proposed to explain self-lofting observed in the aerosols, behavior taken as proof of the presence of smoke. However, self-lofting in sulfate aerosols was observed previously following the Mount Pinatubo eruption (Aquila et al., 2012; Stenchikov et al., 2021), and at the given latitudes a vertical boost would likely be supplied by the upward leg of the Brewer-Dobson circulation. In ACE results, no evidence was found for smoke in the Raikoke southern branch above 17 km. See for example, the results in Figure 3, where the residual spectrum is reproduced extremely well using sulfate aerosol optical constants, with no leftover features in the spectrum that could be attributed to smoke. For the SAGE measurements, sulfate aerosol particles that were larger than anticipated would push the spectral response across the arbitrary threshold chosen to delineate smoke and sulfate aerosols. An update of the Knepp et al. study concluded that the post-Raikoke stratospheric aerosols consisted primarily of unexpectedly large sulfate aerosols rather than smoke particles (https://doi.org/10.5194/amt-15-5235-2022).

There was also no signature of ash observed in the ACE-FTS infrared aerosol spectra. This was determined by the lack of spectral features in the residual spectra that would be associated with volcanic ash, such as silica (Reed et al., 2018). ACE did not start measuring aerosols associated with Raikoke until roughly 2 weeks following the eruption, by which time the ash appears to have settled out (Kloss et al., 2021).

The ACE-FTS is well suited for determining the composition (wt% H_2SO_4) of sulfate aerosols, with high sensitivity resulting from the region near 3,350 cm^{-1} and negligible sensitivity in the analysis to distribution spread. Sulfate aerosols are typically assumed to be 75% H_2SO_4 (Brodowsky et al., 2021), but large deviations from that were observed in the Raikoke aerosol blanket. During the period following the Raikoke eruption, wt% H_2SO_4 varied significantly with time, location, and altitude. The smallest wt% H_2SO_4 observed (in March 2020) was below 50%, and 75% was close to the upper limit for the entire data set. Future studies are planned to investigate possible correlations between wt% H_2SO_4 and H_2O VMR determined from the ACE-FTS.

ACE-FTS measurements extend to high enough wavenumbers to derive information on particle size, but for relatively small particles there is insufficient information to determine both median radius and distribution spread, necessitating fixing one or the other in the analysis, which leads to potentially significant systematic errors in everything except wt% H_2SO_4. More reliable results for particle size and column density could be achieved by exploiting information from the UV/Visible/Near-infrared instrument on the ACE satellite, MAESTRO (Measurement of Aerosol Extinction in the Stratosphere and Troposphere Retrieved by Occultation) (McElroy et al., 2007). A procedure for combining information from the two instruments is under investigation.

Conflict of Interest

The authors declare no conflicts of interest relevant to this study.

Data Availability Statement

ACE-FTS volume mixing ratio and imager retrievals can be accessed at https://databace.scisat.ca/level2/ace_v4.1_v4.2/display_data.php (ACE-FTS Level 2 Data, 2021). First time data users can register at https://databace.scisat.ca/l2signup.php. ACE-FTS infrared aerosol spectra (along with fitted sulfate aerosol spectra) used in the figures are included as Supporting Information S1 and are made available in the University of Waterloo data repository (https://doi.org/10.5683/SP3/X2MJXV).

Acknowledgments
Funding is provided by the Canadian Space Agency (9F045-200575/001/SA) and NASA SAGE-III-ISS Team (80NSSC21K1194).

References

Ansmann, A., Ohneiser, K., Chudnovsky, A., Baars, H., & Engelmann, R. (2021). CALIPSO aerosol-typing scheme misclassified stratospheric fire smoke: Case study from the 2019 Siberian wildfire season. *Frontiers of Environmental Science*, *9*, 769852. https://doi.org/10.3389/fenvs.2021.769852

Aquila, V., Oman, L. D., Stolarski, R. S., Colarco, P. R., & Newman, P. A. (2012). Dispersion of the volcanic sulfate cloud from a Mount Pinatubo–like eruption. *Journal of Geophysical Research*, *117*(D6), D06216. https://doi.org/10.1029/2011JD016968

Bernath, P. F. (2017). The atmospheric chemistry experiment (ACE). *Journal of Quantitative Spectroscopy and Radiative Transfer*, *186*, 3–16. https://doi.org/10.1016/j.jqsrt.2016.04.006

Biermann, U. M., Luo, B. P., & Peter, T. (2000). Absorption spectra and optical constants of binary and ternary Solutions of H_2SO_4, HNO_3, and H_2O in the mid infrared at atmospheric temperatures. *The Journal of Physical Chemistry A*, *104*(4), 783–793. https://doi.org/10.1021/jp992349i

Boone, C. D., Bernath, P. F., Cok, D., Jones, S. C., & Steffen, J. (2020). Version 4 retrievals for the atmospheric chemistry experiment Fourier transform Spectrometer (ACE-FTS) and imagers. *Journal of Quantitative Spectroscopy and Radiative Transfer*, *247*, 106939. https://doi.org/10.1016/j.jqsrt.2020.106939

Boone, C. D., Bernath, P. F., & Fromm, M. D. (2020). Pyrocumulonimbus stratospheric plume injections measured by the ACE-FTS. *Geophysical Research Letters*, *112*(15), 980–989. https://doi.org/10.1029/2020GL088442

Boone, C. D., Walker, K. A., & Bernath, P. F. (2011). An efficient analytical approach for calculating line mixing in atmospheric remote sensing applications. *Journal of Quantitative Spectroscopy and Radiative Transfer*, *247*(6), 106939–106989. https://doi.org/10.1016/j.jqsrt.2010.11.013

Brodowsky, C., Sukhodolov, T., Feinberg, A., Höpfner, M., Peter, T., Stenke, A., & Rozanov, E. (2021). Modeling the sulfate aerosol evolution after recent moderate volcanic activity, 2008–2012. *Journal of Geophysical Research: Atmospheres*, *126*(23), e2021JD035472. https://doi.org/10.1029/2021JD035472

Buijs, H. L., Soucy, M.-A., & Lachance, R. L. (2013). ACE-FTS hardware and level 1 processing. In P. F. Bernath (Ed.), *The atmospheric chemistry Experiment ACE at 10: A solar occultation anthology* (pp. 53–80). A. Deepak Publishing.

Cameron, W., Bernath, P., & Boone, C. (2021). Sulfur dioxide from the atmospheric chemistry experiment (ACE) satellite. *Journal of Quantitative Spectroscopy and Radiative Transfer*, *258*, 107341. https://doi.org/10.1016/j.jqsrt.2020.107341

Chen, W. N., Chiang, C. W., & Nee, J. B. (2002). Lidar ratio and depolarization ratio for cirrus clouds. *Applied Optics*, *41*(30), 6470–6476. https://doi.org/10.1364/AO.41.006470

Christian, K., Wang, J., Ge, C., Peterson, D., Hyer, E., Yorks, J., & McGill, M. (2019). Radiative forcing and stratospheric warming of pyrocumulonimbus smoke aerosols: First modeling results with multisensor (EPIC, CALIPSO, and CATS) views from space. *Geophysical Research Letters*, *46*(16), 10061–10071. https://doi.org/10.1029/2019GL082360

Clarisse, L., Coheur, P.-F., Prata, F., Hadji-Lazaro, J., Hurtmans, D., & Clerbaux, C. (2013). A unified approach to infrared aerosol remote sensing and type specification. *Atmospheric Chemistry and Physics*, *13*(4), 2195–2221. https://doi.org/10.5194/acp-13-2195-2013

Doeringer, D., Eldering, A., Boone, C. D., González Abad, G., & Bernath, P. F. (2012). Observation of sulfate aerosols and SO_2 from the Sarychev volcanic eruption using data from the Atmospheric Chemistry Experiment (ACE). *Journal of Geophysical Research*, *117*(D3), D03203. https://doi.org/10.1029/2011JD016556

Gasteiger, J., & Freudenthaler, V. (2014). Benefit of depolarization ratio at $\lambda = 1064$ nm for the retrieval of the aerosol microphysics from lidar measurements. *Atmospheric Measurement Techniques*, *7*(11), 3773–3781. https://doi.org/10.5194/amt-7-3773-2014

Gilbert, K. L., Turnbull, D. N., Walker, K. A., Boone, C. D., McLeod, S. D., Butler, M., et al. (2007). The onboard imagers for the Canadian ACE SCISAT-1 mission. *Journal of Geophysical Research*, *112*(D12), D12207. https://doi.org/10.1029/2006JD007714

Gordon, I. E., Rothman, L. S., Hill, C., Kochanov, R. V., Tan, Y., Bernath, P. F., et al. (2017). The HITRAN 2016 molecular spectroscopic database. *Journal of Quantitative Spectroscopy and Radiative Transfer*, *203*, 3–69. https://doi.org/10.1016/j.jqsrt.2017.06.038

Gorkavyi, N., Krotkov, N., Li, C., Lait, L., Colarco, P., Carn, S., et al. (2021). Tracking aerosols and SO_2 clouds from the Raikoke eruption: 3D view from satellite observations. *Atmospheric Measurement Techniques*, *14*(12), 7545–7563. https://doi.org/10.5194/amt-14-7545-2021

Guermazi, H., Sellitto, P., Cuesta, J., Eremenko, M., Lachatre, M., Mailler, S., et al. (2021). Quantitative retrieval of volcanic Sulphate aerosols from IASI observations. *Remote Sensing*, *13*(9), 1808. https://doi.org/10.3390/rs13091808

Hofmann, D. J., & Solomon, S. (1989). Ozone destruction through heterogeneous chemistry following the eruption of El Chichón. *Journal of Geophysical Research*, *94*(D4), 5029–5041. https://doi.org/10.1029/JD094iD04p05029

Kanitz, T., Ansmann, A., Foth, A., Seifert, P., Wandinger, U., Engelmann, R., et al. (2014). Surface matters: Limitations of CALIPSO V3 aerosol typing in coastal regions. *Atmospheric Measurement Techniques*, *7*, 2061–2072. https://doi.org/10.5194/amt-7-2061-2014

Kim, M.-H., Omar, A. H., Tackett, J. L., Vaughan, M. A., Winker, D. M., Trepte, C. R., et al. (2018). The CALIPSO version 4 automated aerosol classification and lidar ratio selection algorithm. *Atmospheric Measurement Techniques*, *11*, 6107–6135. https://doi.org/10.5194/amt-11-6107-2018

Kloss, C., Berthet, G., Sellitto, P., Ploeger, F., Taha, G., Tidiga, M., et al. (2021). Stratospheric aerosol layer perturbation caused by the 2019 Raikoke and Ulawun eruptions and their radiative forcing. *Atmospheric Chemistry and Physics*, *21*(1), 535–560. https://doi.org/10.5194/acp-21-535-2021

Knepp, T., Thomason, L., Kovilakam, M., Tackett, J., Kar, J., Damadeo, R., & Flittner, D. (2021). Identification of smoke and sulfuric acid aerosol in SAGE III/ISS extinction spectra following the 2019 Raikoke eruption. [preprint]. Atmospheric Measurement Techniques Discussions. https://doi.org/10.5194/amt-2021-333

Kremser, S., Thomason, L. W., von Hobe, M., Hermann, M., Deshler, T., Timmreck, C., et al. (2016). Stratospheric aerosol—Observations, processes, and impact on climate. *Reviews of Geophysics*, *54*(2), 278–335. https://doi.org/10.1002/2015RG000511

Lund Myhre, C. E., Christensen, D. H., Nicolaisen, F. M., & Nielsen, C. J. (2003). Spectroscopic study of aqueous H_2SO_4 at different temperatures and compositions: Variations in dissociation and optical properties. *The Journal of Physical Chemistry A*, *107*(12), 1979–1991. https://doi.org/10.1021/jp026576n

Ma, Y., Liu, W., Cui, Y., & Xiong, X. (2017). Multiple-scattering effects of atmosphere aerosols on light-transmission measurements. *Optical Review*, *24*(4), 590–599. https://doi.org/10.1007/s10043-017-0352-9

Mayerhofer, T. G., Pahlow, S., & Popp, J. (2020). The Bouguer-Beer-Lambert law: Shining light on the obscure. *ChemPhysChem*, *21*(18), 2029–2046. https://doi.org/10.1002/cphc.202000464

McElroy, C. T., Nowlan, C. R., Drummond, J. R., Bernath, P. F., Barton, D. V., Dufour, D. G., et al. (2007). The ACE-MAESTRO instrument on SCISAT: Description, performance, and preliminary results. *Applied Optics*, *46*(20), 4341–4356. https://doi.org/10.1364/AO.46.004341

Murphy, D. M., Froyd, K. D., Bourgeois, I., Brock, C. A., Kupc, A., Peischl, J., et al. (2021). Radiative and chemical implications of the size and composition of aerosol particles in the existing or modified global stratosphere. *Atmospheric Chemistry and Physics*, *21*(11), 8915–8932. https://doi.org/10.5194/acp-21-8915-2021

Muser, L. O., Hoshyaripour, G. A., Bruckert, J., Horváth, Á., Malinina, E., Wallis, S., et al. (2020). Particle aging and aerosol–radiation interaction affect volcanic plume dispersion: Evidence from the Raikoke 2019 eruption. *Atmospheric Chemistry and Physics*, *20*(23), 15015–15036. https://doi.org/10.5194/acp-20-15015-2020

Niedziela, R. F., Norman, M. L., DeForest, C. L., Miller, R. E., & Worsnop, D. R. (1999). A temperature- and composition-dependent study of H_2SO_4 aerosol optical constants using Fourier transform and tunable diode laser infrared spectroscopy. *The Journal of Physical Chemistry A*, *103*(40), 8030–8040. https://doi.org/10.1021/jp991323o

Ohneiser, K., Ansmann, A., Chudnovsky, A., Engelmann, R., Ritter, C., Veselovskii, I., et al. (2021). The unexpected smoke layer in the High Arctic winter stratosphere during MOSAiC 2019–2020. *Atmospheric Chemistry and Physics*, *21*(20), 15783–15808. https://doi.org/10.5194/acp-21-15783-2021

Oman, L., Robock, A., Stenchikov, G., Schmidt, G. A., & Ruedy, R. (2005). Climatic response to high-latitude volcanic eruptions. *Journal of Geophysical Research*, *110*(D13), D13103. https://doi.org/10.1029/2004JD005487

Osborne, M. J., de Leeuw, J., Witham, C., Schmidt, A., Beckett, F., Kristiansen, N., et al. (2022). The 2019 Raikoke volcanic eruption part 2: Particle phase dispersion and concurrent wildfire smoke emissions. *Atmospheric Chemistry and Physics*, *22*(5), 2975–2997. https://doi.org/10.5194/acp-22-2975-2022

Reed, B. E., Peters, D. M., McPheat, R., & Grainger, R. G. (2018). The complex refractive index of volcanic ash aerosol retrieved from spectral mass extinction. *Journal of Geophysical Research: Atmospheres*, *123*(2), 1339–1350. https://doi.org/10.1002/2017JD027362

Rinsland, C., Yue, G. K., Gunson, M. R., Zander, R., & Abrams, M. C. (1994). Mid-infrared extinction by sulfate aerosols from the Mt. Pinatubo eruption. *Journal of Quantitative Spectroscopy and Radiative Transfer*, *52*(3–4), 241–252. https://doi.org/10.1016/0022-4073(94)90154-6

Sellitto, P., di Sarra, A., Corradini, S., Boichu, M., Herbin, H., Dubuisson, P., et al. (2016). Synergistic use of Lagrangian dispersion and radiative transfer modelling with satellite and surface remote sensing measurements for the investigation of volcanic plumes: The Mount Etna eruption of 25–27 October 2013. *Atmospheric Chemistry and Physics*, *16*(11), 6841–6861. https://doi.org/10.5194/acp-16-6841-2016

Sellitto, P., & Legras, B. (2016). Sensitivity of thermal infrared nadir instruments to the chemical and microphysical properties of UTLS secondary sulfate aerosols. *Atmospheric Measurement Techniques*, *9*(1), 115–132. https://doi.org/10.5194/amt-9-115-2016

Sica, R. J., Izawa, M. R. M., Walker, K. A., Boone, C., Petelina, S. V., Argall, P. S., et al. (2008). Validation of the Atmospheric Chemistry Experiment (ACE) version 2.2 temperature using ground-based and space-borne measurements. *Atmospheric Chemistry and Physics*, *8*(1), 35–62. https://doi.org/10.5194/acp-8-35-2008

Solomon, S., Garcia, R., Rowland, F. S., & Wuebbles, D. J. (1986). On the depletion of Antarctic ozone. *Nature*, *321*(6072), 755–758. https://doi.org/10.1038/321755a0

Stenchikov, G., Ukhov, A., Osipov, S., Ahmadov, R., Grell, G., Cady-Pereira, K., et al. (2021). How does a Pinatubo-size volcanic cloud reach the middle stratosphere? *Journal of Geophysical Research: Atmospheres*, *126*(10), e2020JD033829. https://doi.org/10.1029/2020JD033829

Sun, W., Liu, Z., Videen, G., Fu, Q., Muinonen, K., Winker, D. M., et al. (2013). For the depolarization of linearly polarized light by smoke particles. *Journal of Quantitative Spectroscopy and Radiative Transfer*, *122*, 233–237. https://doi.org/10.1016/j.jqsrt.2012.03.031

Wrana, F., von Savigny, C., Zalach, J., & Thomason, L. W. (2021). Retrieval of stratospheric aerosol size distribution parameters using satellite solar occultation measurements at three wavelengths. *Atmospheric Measurement Techniques*, *14*(3), 2345–2357. https://doi.org/10.5194/amt-14-2345-2021

References From the Supporting Information

Pumphrey, H. C., Glatthor, N., Bernath, P. F., Boone, C. D., Hannigan, J. W., Ortega, I., et al. (2018). MLS measurements of stratospheric hydrogen cyanide during the 2015–2016 El Niño event. *Atmospheric Chemistry and Physics*, *18*(2), 691–703. https://doi.org/10.5194/acp-18-691-2018

Sheese, P. E., Walker, K. A., & Boone, C. D. (2017). A global enhancement of hydrogen cyanide in the lower stratosphere throughout 2016. *Geophysical Research Letters*, *44*(11), 5791–5797. https://doi.org/10.1002/2017GL073519

Yu, P., Toon, O. B., Bardeen, C. G., Zhu, Y., Rosenlof, K. H., Portmann, R. W., et al. (2019). Black carbon lofts wildfire smoke high into the stratosphere to form a persistent plume. *Science*, *365*(6453), 587–590. https://doi.org/10.1126/science.aax1748